ACCEPTED VERSION

Md Julker Nine, Md Ayub, Anthony C. Zander, Diana N. H. Tran, Benjamin S. Cazzolato and Dusan Losic
Graphene oxide-based lamella network for enhanced sound absorption

http://hdl.handle.net/2440/109771

Graphene oxide based lamella network for enhanced sound absorption

Md J. Nine[1,2], Md Ayub[3], Anthony C. Zander[3], Diana N.H. Tran[1,2], Benjamin S. Cazzolato[3], Dusan Losic[1,2]*

[1]School of Chemical Engineering, The University of Adelaide, Adelaide, SA 5005, Australia

[2]ARC Research Hub for Graphene Enabled Industry Transformation, *The University of Adelaide, Adelaide, SA 5005, Australia*

[3]School of Mechanical Engineering, The University of Adelaide, Adelaide, SA 5005, Australia

*Email address: dusan.losic@adelaide.edu.au

Abstract. Noise is an environmental pollutant with recognized impacts on the psychological and physiological health of humans. Many porous materials are often limited by low sound absorption over a broad frequency range, delicacy, excessive weight and thickness, poor moisture insulation, high temperature instability, and lack of readiness for high volume commercialization. Herein we report an efficient and robust lamella-structure as an acoustic absorber based on self-assembled interconnected graphene oxide (GO) sheets supported by a grill-shaped melamine skeleton. The fabricated lamella structure exhibited ~60.3% enhancement over a broad absorption band between 128 Hz and 4000 Hz (~100% at lower frequencies) compared to the melamine foam (MF). The enhanced acoustic absorption is identified to be structure dependent regardless of the density. The sound dissipation in the open-celled structure is due to the viscous and thermal losses, whereas it is predominantly tortuosity in wave propagation and enhanced surface area for the GO-based lamella. In addition to the enhanced acoustic absorption and mechanical robustness, the lamella provides superior structural functionality over many conventional sound absorbers including,

1

moisture/mist insulation, and fire-retardancy. The fabrication of this new sound absorber is inexpensive, scalable and can be adapted for extensive applications in commercial, residential, and industrial building structures.

1. Introduction

Noise is unwanted sound which may be generated from a variety of sources such as domestic appliances (e.g. grinder, vacuum cleaner, dryer), vehicles (e.g. car, bus, train, airplane), industrial plants (e.g. power generator, other machines), and other airborne sources. These sources of noise interfere with communication, and cause annoyance, stress and fluctuations in sleep patterns for humans at normal urban levels leading to higher risk for type-2 diabetes, arterial hypertension, myocardial infarction, and stroke.[1] The World Health Organization (WHO) estimates that per annum loss in terms of disability-adjusted life years (i.e. the number of years lost because of disability) only in Western Europe includes 45,000 years due to noise-induced cognitive impairment in children, 903,000 years due to noise-induced sleep disturbance, 61,000 years due to noise-induced cardiovascular disease, and 22,000 years due to tinnitus.[1-2]

As the awareness of the importance of noise mitigation strategies for public health grows, so does the need to develop new and more effective acoustic absorption materials.[3] It is known that all materials absorb some incident sound as a passive medium however the term "acoustical material" is applied for those high magnitude of sound absorbers. The most efficient acoustic absorptive materials are primarily porous or fibrous, consisting of either inter-connected open, semi-open or closed pore structures with regular or irregular-shapes.[4] These fibrous and porous materials include a wide range of both synthetic (ceramic, metal, and polymer foam, aerogel, Kevlar, fibre glass, glass wool, basalt, carbon nanotubes), and natural (cotton, hemp, coir, ramie, wool, sisal, bamboo, wood, flax, bagasse, jute) substances.[3, 5] To date, numerous structural variations have been reported for efficient acoustic absorption that include cellular,[6] fibrous,[7] granular,[8] membrane,[9] bundled hollow

2

fibre,[10] foam/film layering,[11] nanotubes,[12] and helical shaped porous structures.[13] Among these structures, cellular foam with polymeric, metallic, and ceramic structures have been extensively used as commercial acoustic absorbers due to their ease of handling, installation, replacement, manufacturing, positioning, and durability to provide economical acoustic absorption technology.[3b, 4]

To enhance the acoustic absorption of these cellular and conventional absorptive materials, they have been modified through application of additives (carbon nanotubes (CNTs),[14] textile waste,[15] iron particles,[16] and mica powder[8]) with aims to optimize their structural, thermal and viscous properties. These structural changes with nano to microscale surface modifications provide tunable porosity, tortuosity, and flow resistivity that affect the propagation of sound energy through cellular materials.[17] Although several works have used additional composite fillers to enhance the acoustic absorption by surface modification, such as iron particles for a polyurethane (PU) foam,[16] and CNTs for a PU and silicon foam,[14] there are some negative damping effects attributed to the change of other structural properties (mechanical and thermal) caused by the nanofiller.[18] Verdejo et al.[18] reported a negative damping effect of acoustic absorption in the presence of graphene (0.25 wt%), and CNTs (1 wt%) in free-rising silicone foams, as surface modification by the filler caused a change in the foam structure and increased its stiffness.

Many of commercially used acoustic absorbing materials (such as natural fibres, melamine foams) are hydrophilic by nature and hold moisture in their structure which can possibly lead to bio-deterioration of the material, with significant economic loss for necessary maintenance and replacement.[19] Acoustic absorbers with ineffective moisture insulation can influence the bio-deterioration of the structure that are placed in floors or crawl space,[20] lower parts of walls,[19a] and roofs where water accumulates easily.[19b, 21] Significant moisture and water retention can also reduce acoustic absorption and increase weight of the structure.

3

Furthermore, the strong commercial demands for fire-proof acoustic absorbers limit the use of many natural and synthetic acoustic materials due to their poor fire-retardancy.[22] To overcome the disadvantages of poor fire-retardancy, these fibre-based acoustic materials were often externally modified with halogenated fire-retardants in the past, which have been recognized as global contaminants associated with the adverse health effects on both human and animals.[23] Recently, the ban of halogenated fire-retardants in 2010 has forced industries to look for a new generation of halogen free acoustic absorbers with good fire-retarding properties.[24]

To address the combined challenges achieving enhanced acoustic absorption, mechanical robustness, moisture insulation and fire-retardancy, we have developed a new approach to engineer the internal structure of conventional cellular acoustic absorptive materials using interconnected GO sheets. The concept is based on the creation of unique lamella network using self-assembled GO sheets in a grill-shaped cellular skeleton to create optimal air-flow resistance and tortuosity, which is schematically illustrated in **Figure 1a**. To prove this concept, melamine foam (MF) is chosen as structural support because of its highly porous and well-structured limbs,[25] that interacts well with negatively charged GO and holds self-assembled interconnected films.[26] The self-assembled properties of GO facilitates microscopic sheets (~20 μm^2) to form into a macroscopic film (~0.01 mm^2) providing an edge-to-edge coverage of a large pore of MF that is apparently 500 times greater than the area of GO sheets used. This unique and randomly structured 3D-lamella provide tunable open and closed cell ratios to control the porosity and tortuosity of the structure for excellent noise absorption across broad range of applications. A series of tests were performed to investigate the structural and morphological advantages of the prepared materials for enhanced sound absorption, mechanical stiffness, humidity insulation, and fire-retardancy.

2. Results and Discussion

2.1. Structural Characterisations

Typical structure of MF before and after the formation of lamella is presented in **Figure 1a** and **Figure S3**. (Detailed information regarding chemical analysis of the structure has been discussed in supporting information file) The self-assembly of microscopic GO sheets (~20 μm^2) forming into the macroscopic film and *in-situ* limb-to-limb connection have been observed after a low temperature curing process as shown in **Figure 1b**, in which the GO in semi-liquid phase starting to connect physically during the evaporation of water. Cross sectional SEM images made across vertical and horizontal directions showed the self-assembled GO film connected to the melamine limbs in the grill-shaped skeleton which covered an approximate area of ~0.01 mm^2 as shown in **Figure 1c-e** and **Figure S6**. The density of lamella structures based on the self-assembly of GO sheets into the MF skeleton is tunable by loading of different concentrations of nematic-GO. The SEM images of MFGO lamella structures prepared with various densities (~10 to 25 kg/m^3) are shown in **Figure 1f-i**. Images confirm the increase in density is related to the increase in the number of closed cells in the porous skeleton that reached to a critical state at a density of 24.12 kg/m^3 (**Figure S5 a-c**). Further increases in the density by increasing the loading of GO deformed the porous structure in size and shape after curing as shown in **Figure S5 d, e**, which was attributed to the ultimate inner tension during the *in-situ* film formation of GO, hence 24.12 kg/m^3 has been considered as the critical mass density for desirable micro structures. In addition to the deformation, the enhanced loading of nematic-GO in the structure also created a fully closed outer shell covering the entire melamine skeleton as shown in **Figure S5f**, which was not a desirable structure for acoustic applications. Moreover, the homogeneity and regularity of GO distribution can also be observed in **Figure S5g** that greatly depended on the GO concentration with homogeneous loading and the subsequent drying method (with and without squeezing). For clarity, the MFGO samples with the different densities (12.39, 15.68,

18.77, 21.41 and 24.12 kg/m^3) will be denoted as MFGO-1, MFGO-2, MFGO-3, MFGO-4, and MFGO-5, respectively, while the control melamine sample is denoted as Control-MF.

2.2. Mechanical Robustness and Compressibility of the Structure

To explore mechanical strength of GO assisted lamella structures, their mechanical properties during both static and dynamic compression tests were performed for different MFGO structures compared to the Control-MF. The results clearly indicate that the increase in GO loading increased the mechanical strength of the samples as shown in **Figure 2**. The sample with a density of 24.12 kg/m^3 could support at least 3,500 times its own weight (500 g), as shown in **Figure 2b**, while the Control-MF was flattened with approximately 90% compression subjected to the identical load. Load carrying capability of the structure increased with the increase in GO density, where the sample MFGO-5 showed maximum static loading capacity of ~10 kPa with a negligible mechanical deformation.

To provide more precise measurements under a dynamic load, a cyclic compression test was performed using a micro-compression tester as shown in **Figure 2c**. The MFGO samples with higher densities exhibited increased stiffness, while undergoing a compression of 80% of their length. The recovery to their original shape was fast when compressed to a strain of 40%. The higher density samples generated superior stiffness, but lowered the recovery rate at increased compression percentage. The effect of interconnected lamella shows linear compressional stress before undergoing permanent deformation or collapse in the melamine skeleton. The calculated elastic modulus of the lamella structure in MFGO-1, MFGO-3 and MFGO-5 are 4.68 kPa, 7.17 kPa and 13.46 kPa, respectively, which are obtained from the tangent of the curves in elastic zone (linear) of the compressional stress-strain curve as shown in **Figure 2c**. The observed enhanced mechanical strength can be attributed to the randomly aligned GO sheets in the structure (**Figure S6**). The mechanical compression and fast recovery under finger press has also been shown in **Figure 2d** and **movie S1** to demonstrate the improved

6

mechanical properties compared with Control-MF. The robustness and mechanical compressibility achieved in this work is found to be comparable to other 3D structures made with the incorporation of graphene derivatives reported elsewhere.[27]

2.3. Acoustic Absorption of MFGO and MFrGO Lamella Structures

The acoustic absorption performances of the Control-MF, MFGO and the reduced-MFGO (MFrGO) samples were studied for normal incidence sound propagation. The experimental results for the acoustic activity (α) and corresponding air flow-resistance of the samples were measured for different thickness and densities as tabulated in **Table S1**. Thickness and density dependent acoustic absorption behaviour as a function of frequency (128 Hz-4000 Hz) have been displayed in **Figure 3**. The Control-MF samples with thickness between 6.5 ± 0.5 mm and 26 ± 0.5 mm exhibited typical behaviour of flexible open cell foams, i.e., a linear increase in the absorption coefficient with the increase of frequency (**Figure 3a**). This behaviour is commonly observed in open cell melamine and polyurethane foams.[28] For comparison, the MFGO-1 (12.39 kg/m^3) sample with various thicknesses showed the thickness dependence enhanced absorption coefficient as shown in **Figure 3a**. Additional shearing resonances have also been observed for relatively thicker samples, which can be attributed to the edge constraints of the slightly large samples used in the impedance tube. The similar resonance behaviour can also be found in literature, that is sometimes resolved by constraining the motion of such elastic frames using needles.[29]

In our experiment, it was observed that the incorporation of the self-assembled-GO lamella can significantly reduce the resonance effect at high density (higher loading). The increase in the mass associated with density appears to lower the resonance frequency, however, the simultaneous increase in stiffness with the increase in density moves the resonance towards higher frequencies, which eventually makes the resonances disappeared at high density samples as shown in **Figure 3b**. The disappearance of this resonance behaviour might be

caused by the mechanical stiffness achieved by the integration of GO in the MF skeleton that restricts the frame's motion.[30] Moreover, a significantly improved absorption coefficient with an interesting high absorption pattern toward low frequency spectrum has been observed for the higher density sample at a constant thickness of 26 ± 0.5 mm.

In the second series of experiments as demonstrated in **Figure 3b,** the density dependent sound absorption of MFGO structures was compared with the Control-MF using the same thickness (26 ± 0.5 mm). An interesting phenomenon is observed in the higher density of MFGO that shifts the absorption curve peak towards the lower frequencies, which causes the peak of the sound absorption coefficients to spread over a broad frequency spectrum range between 1000 Hz and 4000 Hz. The link between acoustic activity over the measured frequency spectrum and loading of GO (density) into MF is presented in **Figure 3c**, showing an almost linear increase in acoustic activity with the increase in loading percentage of GO. The density of the initial Control-MF foam (9.84 kg/m^3) was increased to 24.12 kg/m^3, after a maximum GO loading in its unaffected structure.

The normalised acoustic impedance (by the characteristic impedance of the air) has also been obtained from the measured acoustic data for the Control-MF, MFGO samples with different densities. The real and imaginary part of the impedance are shown in **Figure S7**, where the real part indicates the resistance associated with acoustic energy losses and the imaginary part corresponds to the reactance associated with phase changes between the acoustic pressure and velocity.[31] It can be seen that the value of the real part of the normalised acoustic impedance is reduced at low frequency with the increase in the sample density, which results in the increased absorption for high density samples. Similarly, a shift in the value of the imaginary part of the impedance towards the low frequency can be observed with the increase of the lamella density.

The reduced density with the unchanged physical structures were studied to investigate whether the acoustic absorption coefficient of the materials is affected mostly by structural variation or their density. To observe the effect of density variation for uniform physical structure, we selected two samples (MFGO-3 (18.77 kg/m^3) and MFGO-5 (24.12 kg/m^3)) to compare with their reduced version (MFrGO-3 and MFrGO-5) for a constant thickness 26 ± 0.5 mm. The density of the MFGO samples were reduced significantly from 18.77 kg/m^3 (MFGO-3) to 14.81 kg/m^3 (MFrGO-3), and 24.12 kg/m^3 (MFGO-5) to 18.09 kg/m^3 (MFrGO-5) due to loss of oxygen functional groups and moisture in the GO structure as shown in **Figure S2d** and **S4a**. However, the reduction did not change the physical structure of lamella as can be observed in **Figure S4b, c**. The reduced sample of MFrGO-3 and MFrGO-5 (26 ± 0.5 mm) showed a sound absorption trend similar to the non-reduced MFGO-3 and MFGO-5 (26 ± 0.5 mm) with no significant changes in the acoustic absorption peaks as presented in **Figure 3d**. The change in acoustic activity over the broad frequency range from 128 Hz to 4000 Hz is also negligible, which is 0.720 for MFGO-3 sample to 0.698 for MFrGO-3 and 0.787 for MFGO-5 and 0.771 for MFrGO-5. The results confirmed that the change in density of the sample does not affect the absorption coefficient if the micro-structure of the sample remains unchanged.

The comparative normalized acoustic activity, which provides a single measure of the absorption over a broad frequency range, of Control-MF, MFGO and MFrGO structures are tabulated in **Table S1**. The absorption coefficient for MFGO-5 and MFrGO-5 reached its maxima near 1100 Hz and remained almost steady for the rest of the frequency spectrum (**Figure 3d**), which can be considered as one of best acoustic absorbers, capable of outperforming other low-density porous acoustic absorbers. Humans are most responsive to sounds between 1,000 and 5,000 Hz, and are not likely to hear very low or very high frequencies unless they are intense as a function of frequency. The samples, in this experiment, show a clear absorption peak over the broad range of 1000–4000 Hz, where

human sensitivity to noise is high.[32] The sound absorption coefficient of this new GO-based lamella structure has been compared with other commercial acoustic absorber as listed in **Table 1**.

Table 1: Comparison of octave-band acoustic absorption coefficient for our materials with other commercial acoustic absorbers used in building structures.[6a, 15, 33]

Materials	Density kg/m^3	Thickness (mm)	Acoustic absorption coefficient			
			500 Hz	1000 Hz	2000 Hz	4000 Hz
MFGO-5 (Experiment)	24.12	26	0.38	0.82	0.98	1.0
MFrGO-5 (Experiment)	18.09	26	0.34	0.79	0.98	0.90
Melamine foam (Experiment)	9.84	26	0.22	0.42	0.62	0.83
Polyurethane foam	37.4	40	0.06	0.84	0.15	~0.21
Aluminum foam	9320	20	0.13	0.22	~0.52	--
Wood	--	16	0.10	0.09	0.08	0.07
Cocos fibre roll felt	--	29	0.22	0.35	0.47	0.57
Acoustical plaster	350	25	0.66	0.65	0.62	0.68
Rock wool	80	50	0.92	0.90	0.88	0.88
Mineral wool (in front of wall)	70	50	0.65	0.60	0.75	0.65
Perforated veneered Chipboard (ø = 1 mm, 9 % hole)	--	50	0.58	0.59	0.68	0.35
Natural coir fiber	153	30	0.28	0.84	0.73	0.82

As can be seen in **Figure 3b**, the normal incident sound absorption co-efficient is doubled with the highest density (MFGO-5) sample at some frequencies. The overall percentage enhancement in absorption activity for different density of MFGO and MFrGO samples with

26 ± 0.5 mm are presented in **Figure 4a** showing a maximum of ~60.3 % enhancement for the MFGO-5 sample. The percentage enhancement of acoustic activity has been identified to be structure dependent for a specific sample with constant thickness but different densities. Conversely, samples of different densities with unchanged internal structure do not have significant effect on the acoustic absorption performance.

The flow resistivity was measured for these newly developed samples to investigate the influence of lamella in the structure to understand acoustic propagation through the materials. The changes in flow resistance for different density samples before and after reduction compared to the open cell Control-MF are presented in **Figure 4b**. As expected, the flow resistance increased as the sample density increases, which is caused by the increased number of lamella in the structure. The measured flow resistivity of the highest density lamella structure (MFGO-5) was found approximately 40932 Ns/m^4 which is about four times higher than that of Control-MF (~10450 Ns/m^4). The measured flow resistivity of Control-MF is in a good agreement with the previous literature.[25] The reduced density samples (MFrGO-3 and MFrGO-5) did not show much difference in flow resistivity compared to non-reduced samples (MFGO-3 and MFGO-5) since the reduction process did not affect their internal physical structures. The results again are in good agreement that the structural parameters (porosity, tortuosity, and blockage) are more important than the density to achieve higher acoustic absorption within the sample.

The outstanding sound absorption performance and the elimination of shearing resonances of these new structures are principally attributed to the air-flow resistance developed by the GO-based lamella structures, and improved stiffness of the Control-MF porous skeleton, respectively. The air flow resistance is governed by the structural properties of absorption material (**Figure 4c**) which includes porosity, pore size, tortuosity and thickness. For instance, an open cell structure with lower porosity, smaller pore size and greater thickness generally possesses higher air flow resistance and vice versa. Hence, for a given porosity and thickness,

the flow resistance increases with decreasing pore size of the foam skeleton. In the case of the MFGO samples, the interconnected GO thin film randomly blocks the pores inside the melamine skeleton (**Figure 4c**), which changes the wave propagation path and thus significantly increases the tortuosity and slightly reduces the porosity of the material. This results in the increased flow resistance exhibited by all MFGO and MFrGO structures. In addition, the interconnected GO films shrink the pores creating internal tension during the curing process, which thereby constrains the motion of its elastic frame and enhances the stiffness of the material. The in-plane stiffness is also extremely high relative to the melamine skeleton. This causes the resonance frequency to shift towards higher frequency and eventually moves the resonances outside the frequency range of interest. Hence, the GO lamella structures in this study possessed high airflow resistance and correspondingly exhibited the enhanced acoustic absorption which is much higher than that of open cell structures. Absorbing materials are passive mediums that lower noise by converting coherent pressure variation it into heat. Acoustic absorption depends on the frequency of sound waves. In porous materials, at high frequencies an adiabatic process takes place that produces heat loss due to friction when the sound wave crosses the irregular pores. On the other hand, at low frequencies, elastic porous materials absorb sound by the energy loss caused by heat exchange which is an isothermal process.[4]

2.4. Enhanced Moisture Insulation and Fire-retardant Properties

Sound absorbing materials when incorporated into building structures have a high requirement to provide the moisture insulation and fire-retardant properties, which is one of the challenges to meet for commercial acoustic absorbers. In general, MF and GO are hydrophilic and prone to moisture entrapment in the structure, which may have negative impacts on the building structure, such as the growth of moulds and fungi in highly humid conditions.[19a] Therefore, MFGO samples were reduced to not only achieve superior moisture

insulation, and fire-retardancy but also to reduce its weight in the reduction process to make the structure both light as well as highly stable.[34] The reduced MFGO (MFrGO) samples exhibited outstanding moisture repellent properties, light weight (density reduction) and fire-retardant properties as shown in **Figure 5**.

The hydrophilic melamine skeleton with the inclusion of GO showed enhanced water contact angle of CA~104°, which further became superhydrophobic (super water repellent) showing a water contact angle of ~155° after the reduction process of the structure as shown in **Figure 5a** and **Movie S2**. The self-assembly of GO lamella sheets in the MF structure enables it to resist moisture penetration by creating an impermeable barrier layer. Hence, the analysis of moisture absorption and desorption of the MFGO-3, and MFGO-5 samples including their reduced derivatives revealed excellent moisture insulation that provided almost 4-5 times better moisture insulation compared to Control-MF as shown in **Figure 5b**. The superhydrophobic MFrGO samples outperform Control-MF and MFGO samples in both the absorption and desorption cycle (**Figure 5b, c**).

Finally the thermal stability and flammability of the two representative samples (MFGO-3 and MFrGO-3) were investigated compared with Control-MF. The reduction of GO in MFrGO-3 sample showed higher thermal stability in comparison to the Control-MF and GO modified sample (MFGO-3) as shown in **Figure S8**. The thermogravimetric analysis of the samples showed that MFGO-3 sample lost mass in two stages between 150 °C and 400 °C, whereas only a single step mass loss was identified for MFrGO-3 sample at 350 °C. The thermal instability of non-reduced MFGO-3 samples was due to the abundant oxygen functional groups in the structure that was reduced to provide structural stability, which is also been confirmed by the volume of residue left after combustion as shown in **Figure S9**. Moreover, the use of GO without further reduction was found to possess an explosive fire hazard due to its possible flammability as shown in **Figure S10**.[34] The self-explosive behaviour of GO film was mitigated by reduction of MFGO lamella structure for enhanced

stability during fire as shown in **Figure 5** and **Movie S3**. Therefore, the MFrGO samples are optimal acoustic absorber with high low density, high thermal stability and enhanced sound absorption.

3. Conclusion

A novel approach to create a robust and low-density lamella using self-assembled nematic-GO in melamine foam has been demonstrated for high performance acoustic absorption. The self-assembled GO-films were found well interconnected with the limbs of the melamine skeleton that resulted in the optimal airflow resistance, tortuosity against sound wave propagation and internal reflection hence shows enhanced acoustic absorption. The formation of this interconnected GO-based lamella can be universal for any supporting cellular structures of polymers, ceramics, and metals. The reported structures also displayed moisture insulation and fire-retardant properties that significantly reinforce its functionality to be used in adverse environments including high humidity, under water and fire risks conditions. Most importantly, about 60 % enhancement in broad-band acoustic absorption (>100% at low frequencies) has been determined for this new structure which is significantly higher than many other commercial sound-absorbing materials. The enhancement of acoustic absorption has been identified to be structure dependent regardless of density. The performance of this multifunctional material for broadband acoustic absorption with inexpensive scalable production suggests significant potential for practical applications in noise mitigation of residential and industrial building structures as well as for transportation systems.

4. Materials and Method

Synthesis of GO. Graphite flakes (<45 μm) were chemically exfoliated following the improved Hummers method.[35] The complete reaction was performed using a 9:1 ratio of H_2SO_4/H_3PO_4 (360:40 ml) with 18 g of $KMnO_4$ for the oxidation of 3 g of graphite flakes. The exfoliation was carried out at 50 °C while stirring for 12 h. The solution was then cooled

to room temperature and poured onto ice cubes (300 ml) with 3 ml of 30% H_2O_2. Finally, the mixture was repeatedly centrifuged at 4000 rpm for 2 h for washing with distilled water (twice), 32% of HCl (twice) and ethanol (twice) respectively to obtain GO, which was stored as concentrated aqueous solution (2-5 mg/ml).

Preparation of GO Assisted Lamella Structure with Melamine foam. The as-received melamine foam was cut into pieces with a round sharp-edged punch of 26.5 mm in diameter to be set in the impedance tube. The thickness of the samples was varied between 6 mm to 26.5 mm. The highly stable nematic phase of aqueous GO were used to load into melamine skeleton. The pieces of melamine foam soaked into dimethylformamide (DMF) before dipping into the aqueous GO for easy access of GO into the open cell-network for homogeneous distribution. Finally, the MF filled with homogenously distributed GO were dried at 50 °C in an oven for 12 hrs. The loading percentage was controlled by using a different concentration for GO and repetition of the cycle to obtain different densities of MFGO samples. The MFGO samples with different densities were reduced in two steps to observe the change in relevant properties of the lamella structure which includes weight, density, and wettability of the structure. The step-1 involves reduction of the MFGO samples using hydrazine vapor followed by the step-2 of thermal annealing at 160 °C in a vacuum oven for 6 hrs. The MFGO samples of different densities (i.e MFGO-3, MFGO-5) were named as MFrGO (i.e MFrGO-3, MFrGO-5) in the literature after their reduction.

Supporting Information

Supporting Information is available from the Wiley Online Library or from the author.

References.

[1]   T. Münzel, T. Gori, W. Babisch, M. Basner, *European Heart Journal* **2014**, 35, 829.
[2]   World Health Organization, Copenhagen 2011.
[3]   a) J. P. Arenas, M. J. Crocker, *Sound & vibration* **2010**, 44, 12; b) X. Zhu, B.-J. Kim, Q. Wang, Q. Wu, *Recent Advances in the Sound Insulation Properties of Bio-based Materials*, **2013**.
[4]   X. Sagartzazu, L. Hervella-Nieto, J. M. Pagalday, *Archives of Computational Methods in Engineering* **2008**, 15, 311.
[5]   M. Ayub, A. C. Zander, C. Q. Howard, B. S. Cazzolato, D. M. Huang, V. N. Shanov, N. T. Alvarez, *Applied Acoustics* **2017**, 127, 223.
[6]   a) T. J. Lu, F. Chen, D. He, *The Journal of the Acoustical Society of America* **2000**, 108, 1697; b) Y. Li, Z. Li, F. Han, *Procedia Materials Science* **2014**, 4, 187.
[7]   J. Zhu, J. Sun, H. Tang, J. Wang, Q. Ao, T. Bao, W. Song, *Powder Technology* **2016**, 301, 1235.
[8]   L. Lapčík, M. Vašina, B. Lapčíková, E. Otyepková, K. E. Waters, *Composites Part B: Engineering* **2015**, 77, 304.
[9]   C. M. Wu, M. H. Chou, *European Polymer Journal* **2016**, 82, 35.
[10]   Y. J. Qian, D. Y. Kong, Y. Liu, S. M. Liu, Z. B. Li, D. S. Shao, S. M. Sun, *Applied Acoustics* **2014**, 82, 23.
[11]   X. Sun, W. Liang, *Composites Part B: Engineering* **2016**, 87, 21.
[12]   M. Ayub, A. C. Zander, C. Q. Howard, D. M. Huang, B. S. Cazzolato, *Journal of Computational Acoustics* **2015**, 23, 1540012.
[13]   B.-S. Kim, S.-J. Cho, D.-k. Min, J. Park, *Composite Structures* **2016**, 145, 242.
[14]   a) S. Basirjafari, R. Malekfar, S. E. Khadem, *Journal of Applied Physics* **2012**, 112, 104312; b) R. Verdejo, R. Stämpfli, M. Alvarez-Lainez, S. Mourad, M. A. Rodriguez-Perez, P. A. Brühwiler, M. Shaffer, *Composites Science and Technology* **2009**, 69, 1564.
[15]   A.-E. Tiuc, H. Vermeşan, T. Gabor, O. Vasile, *Energy Procedia* **2016**, 85, 559.
[16]   F. Scarpa, W. A. Bullough, P. Lumley, *Proceedings of the Institution of Mechanical Engineers, Part C: Journal of Mechanical Engineering Science* **2004**, 218, 241.
[17]   A. JF., Elsevier Applied Science London **1993.**, Ch. 11.
[18]   R. Verdejo, C. Saiz-Arroyo, J. Carretero-Gonzalez, F. Barroso-Bujans, M. A. Rodriguez-Perez, M. A. Lopez-Manchado, *European Polymer Journal* **2008**, 44, 2790.
[19]   a) H. Viitanen, J. Vinha, K. Salminen, T. Ojanen, R. Peuhkuri, L. Paajanen, K. Lähdesmäki, *Journal of Building Physics* **2009**, 33, 201; b) S. Dedesko, J. A. Siegel, *Microbiome* **2015**, 3, 71.
[20]   J. Richter, K. Staněk, *Energy Procedia* **2015**, 78, 2754.
[21]   M. Piotrowska, A. Otlewska, K. Rajkowska, A. Koziróg, M. Hachułka, P. Nowicka-Krawczyk, G. J. Wolski, B. Gutarowska, A. Kunicka-Styczyńska, A. Żydzik-Białek, *PLOS ONE* **2014**, 9, e109402.
[22]   S. Fatima, A. R. Mohanty, *Applied Acoustics* **2011**, 72, 108.
[23]   a) M. Alaee, P. Arias, A. Sjödin, Å. Bergman, *Environment International* **2003**, 29, 683; b) S. Shaw, in *Reviews on Environmental Health*, Vol. 25, 2010, 261.
[24]   a) J. DiGangi, A. Blum, Å. Bergman, C. A. de Wit, D. Lucas, D. Mortimer, A. Schecter, M. Scheringer, S. D. Shaw, T. F. Webster, *Environmental Health Perspectives* **2010**, 118, A516; b)

M. J. Nine, D. N. H. Tran, T. T. Tung, S. Kabiri, D. Losic, *ACS Applied Materials & Interfaces* **2017**, 9, 10160.

[25]   N. Kino, T. Ueno, *Applied Acoustics* **2008**, 69, 325.

[26]   a) M. J. Nine, M. A. Cole, D. N. H. Tran, D. Losic, *Journal of Materials Chemistry A* **2015**, 3, 12580; b) M. J. Nine, T. T. Tung, D. Losic, in *Comprehensive Supramolecular Chemistry II*, DOI: https://doi.org/10.1016/B978-0-12-409547-2.12634-4, Elsevier, Oxford **2017**, p. 47.

[27]   a) J. Li, J. Li, H. Meng, S. Xie, B. Zhang, L. Li, H. Ma, J. Zhang, M. Yu, *Journal of Materials Chemistry A* **2014**, 2, 2934; b) P. K. Sahoo, R. Aepuru, H. S. Panda, D. Bahadur, *Scientific Reports* **2015**, 5, 17726; c) K. H. Kim, Y. Oh, M. F. Islam, *Nat Nano* **2012**, 7, 562; d) H. Lu, C. Li, B. Zhang, X. Qiao, C.-Y. Liu, *RSC Advances* **2016**, 6, 43007.

[28]   a) F. Scarpa, F. C. Smith, *Journal of Intelligent Material Systems and Structures* **2004**, 15, 973; b) A. M. M. William O. Hughes, Mark E. McNelis, in *Aerospace Testing Seminar; 28th; 25-27 Mar. 2014; Los Angeles, CA; United States*, 2014.

[29]   W. Li, *Master's Thesis*, University of Kentucky, Theses and Dissertations--Mechanical Engineering. 48, **2014**.

[30]   C. Wassilieff, *Applied Acoustics* **1996**, 48, 339.

[31]   R. Maderuelo-Sanz, J. M. Barrigón Morillas, M. Martín-Castizo, V. Gómez Escobar, G. Rey Gozalo, *Latin American Journal of Solids and Structures* **2013**, 10, 585.

[32]   S. Subramonian, L. Remy, D. Schroer, *Cellular polymers* **2004**, 23, 349.

[33]   a) M. Vorländer, *Auralization: fundamentals of acoustics, modelling, simulation, algorithms and acoustic virtual reality*, Springer Science & Business Media, **2007**; b) M. Hosseini Fouladi, M. Ayub, M. Jailani Mohd Nor, *Applied Acoustics* **2011**, 72, 35.

[34]   H. Turgut, Z. R. Tian, F. Yu, W. Zhou, *The Journal of Physical Chemistry C* **2017**, 121, 5829.

[35]   a) D. C. Marcano, D. V. Kosynkin, J. M. Berlin, A. Sinitskii, Z. Sun, A. Slesarev, L. B. Alemany, W. Lu, J. M. Tour, *ACS Nano* **2010**, 4, 4806; b) W. S. O. Hummers, R. E. , *J. Am. Chem. Soc.* **1958**, 80, 1339; c) M. J. Nine, D. N. H. Tran, A. ElMekawy, D. Losic, *Carbon* **2017**, 117, 252.

Figure captions:
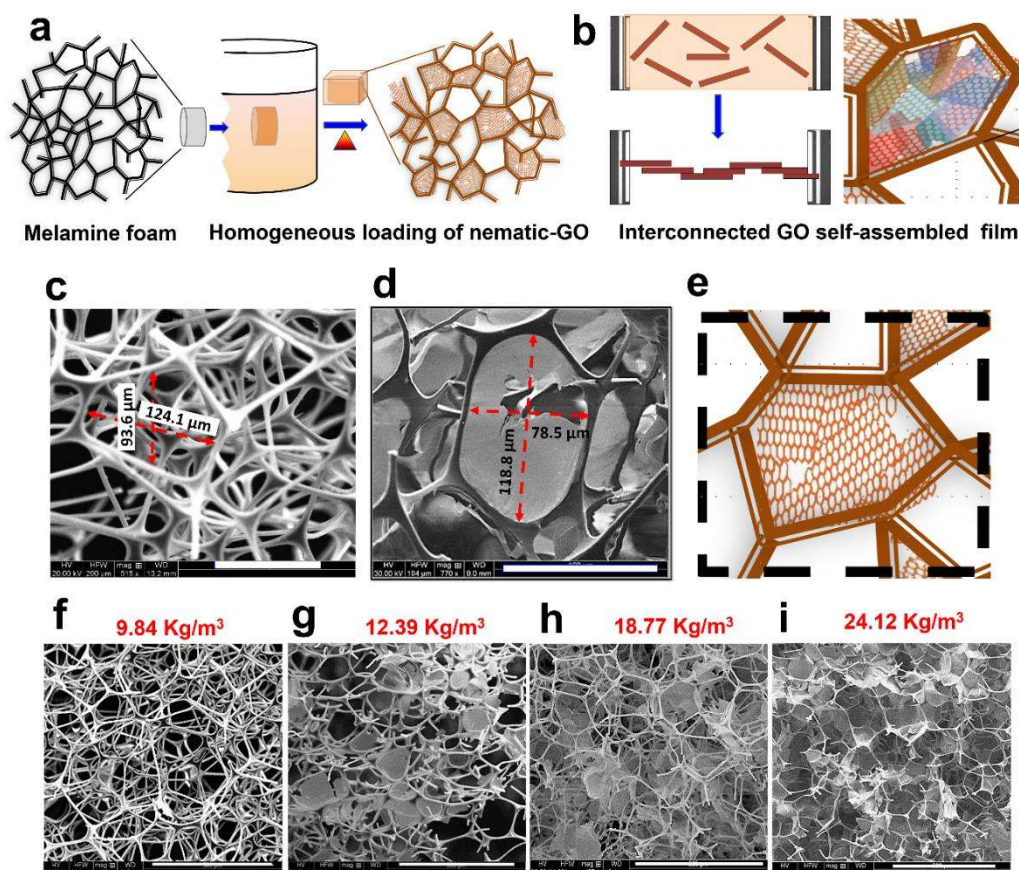
Figure 1. Synthesis of GO assisted lamella structure with tunable densities. a) Schematic presentation of synthesised GO-lamella structure in melamine skeleton. b) Self-assembly of microscopic GO sheets to form macroscopic interconnected GO film. c) Lateral distance between limbs of the melamine skeleton. d-e) Self-assembled interconnected GO film in MF cell and schematic of the macroscopic GO film forming a close cell. f) SEM of Control-MF skeleton with a density of 9.84 kg/m^3. g) Cross-section of MFGO-1 at a density of 12.39 kg/m^3. h) Cross-section of MFGO-3 at a density of 18.77 kg/m^3. i) Cross-section of MFGO-5 at a density of 24.12 kg/m^3. Scale bar of c-d are 100 µm and f-i are 500 µm.
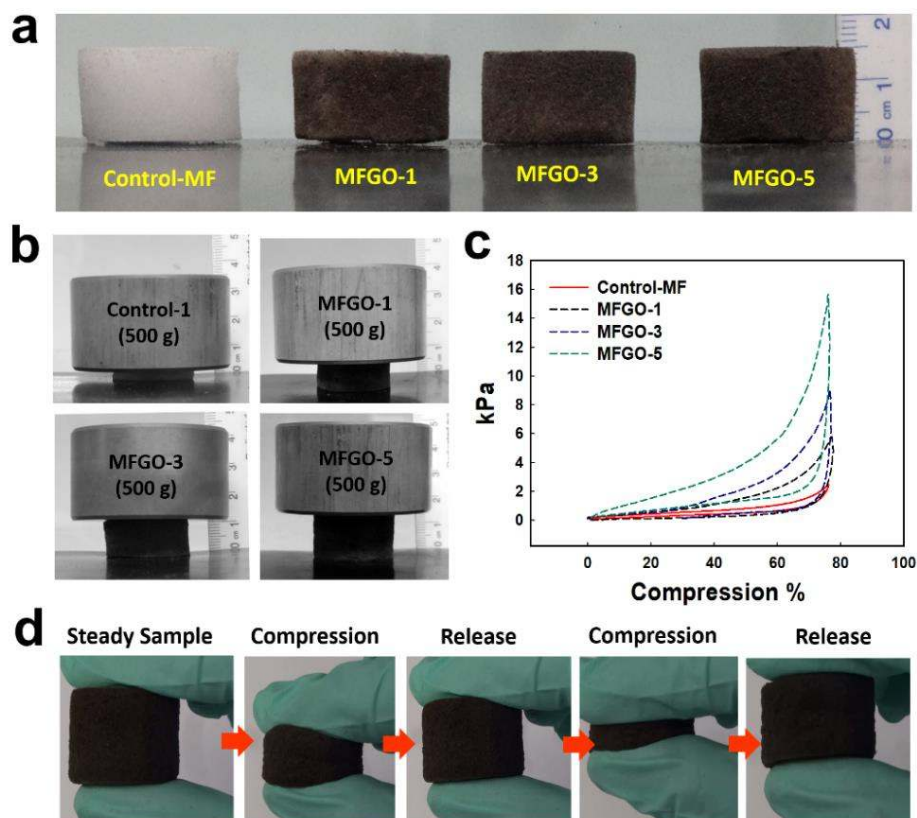
Figure 2. Mechanical properties of MFGO structures. a) Digital photograph of a Control-MF and MFGO of different densities prepared using different GO loadings. b) Static load of 500 g applied to the samples to observe the enhanced mechanical strength. c) Comparative compression cycles of the samples (Control-MF, MFGO-1, MFGO-3 and MFGO-5). d) Compressibility and recovery by simple finger press.
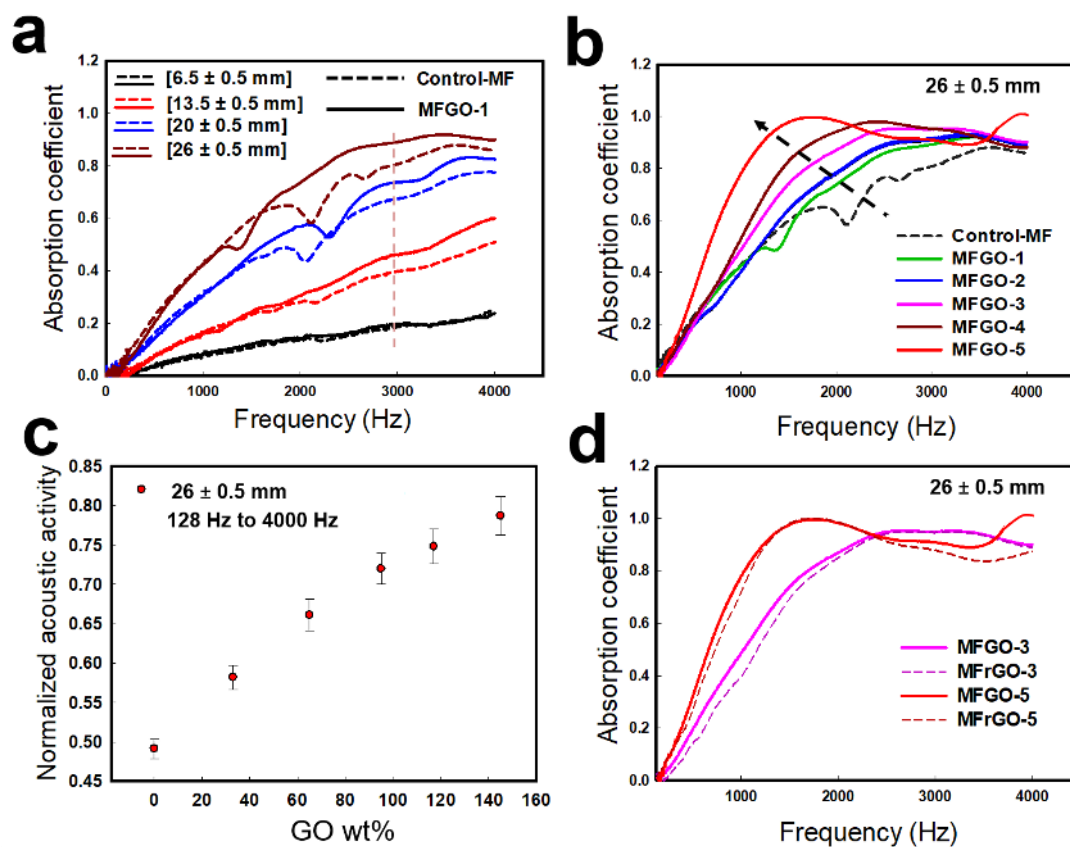
Figure 3. Acoustic properties of Control-MF, MFGO and MFrGO samples. a) Thickness dependent acoustic absorption of MFGO-1 (12.39 kg/m^3) samples compared to Control-MF. b) Acoustic absorption of MFGO samples of 5 different densities from 12.39 kg/m^3 to 24.12 kg/m^3 compared to Control-MF for a thickness of 26 ± 0.5 mm. c) Normalized acoustic activity based on GO loading %. d) Comparative acoustic absorption coefficient as a function of frequency before and after reduction of 2 different density lamella structures (MFGO-3 and MFGO-5).
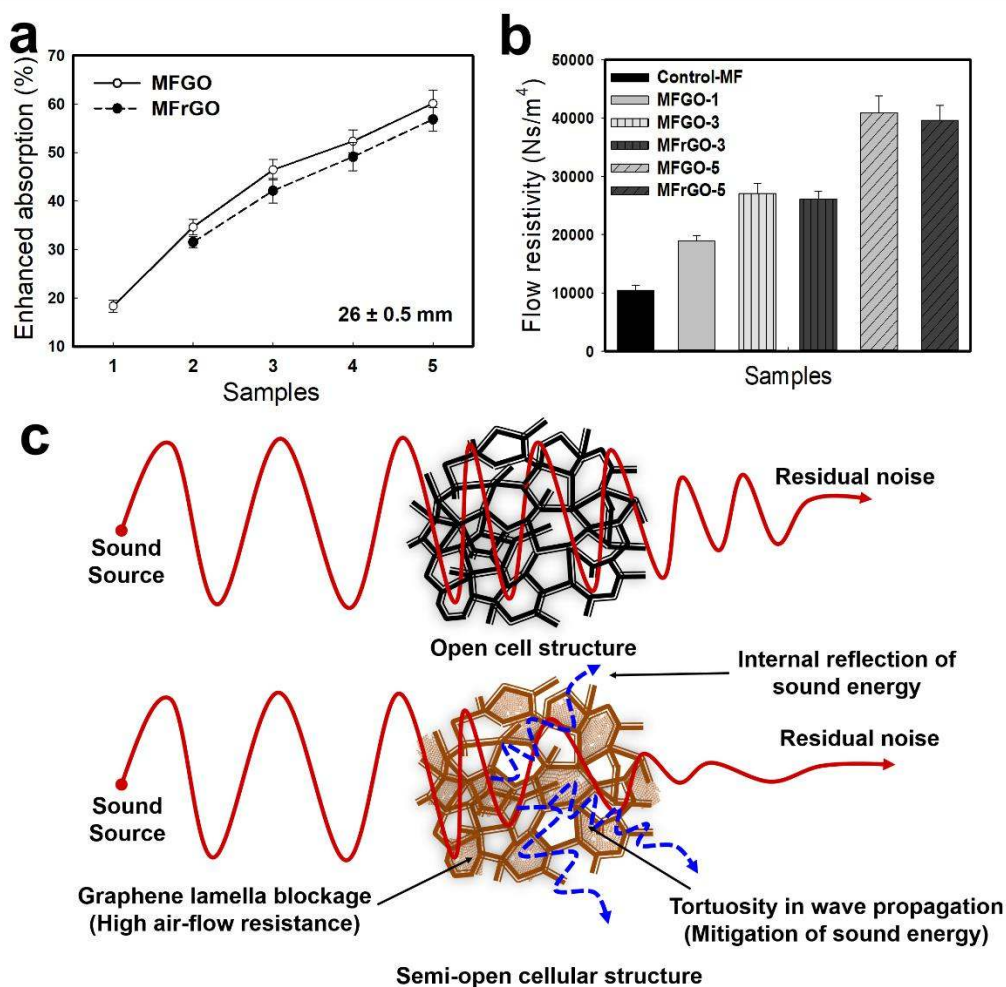
Figure 4. Performance enhancement and absorption mechanism. a) The enhancement (%) of acoustic absorption of lamella structures for both MFGO and MFrGO samples (26 mm thickness) compared to control-MF. b) Enhanced flow resistivity of different density lamella structures (MFGO-1, MFGO-3, MFrGO-3, MFGO-5 and MFrGO-5) compared to Control-MF. c) Schematic of acoustic propagation through open cell MF structure and semi-open cell lamella structures.
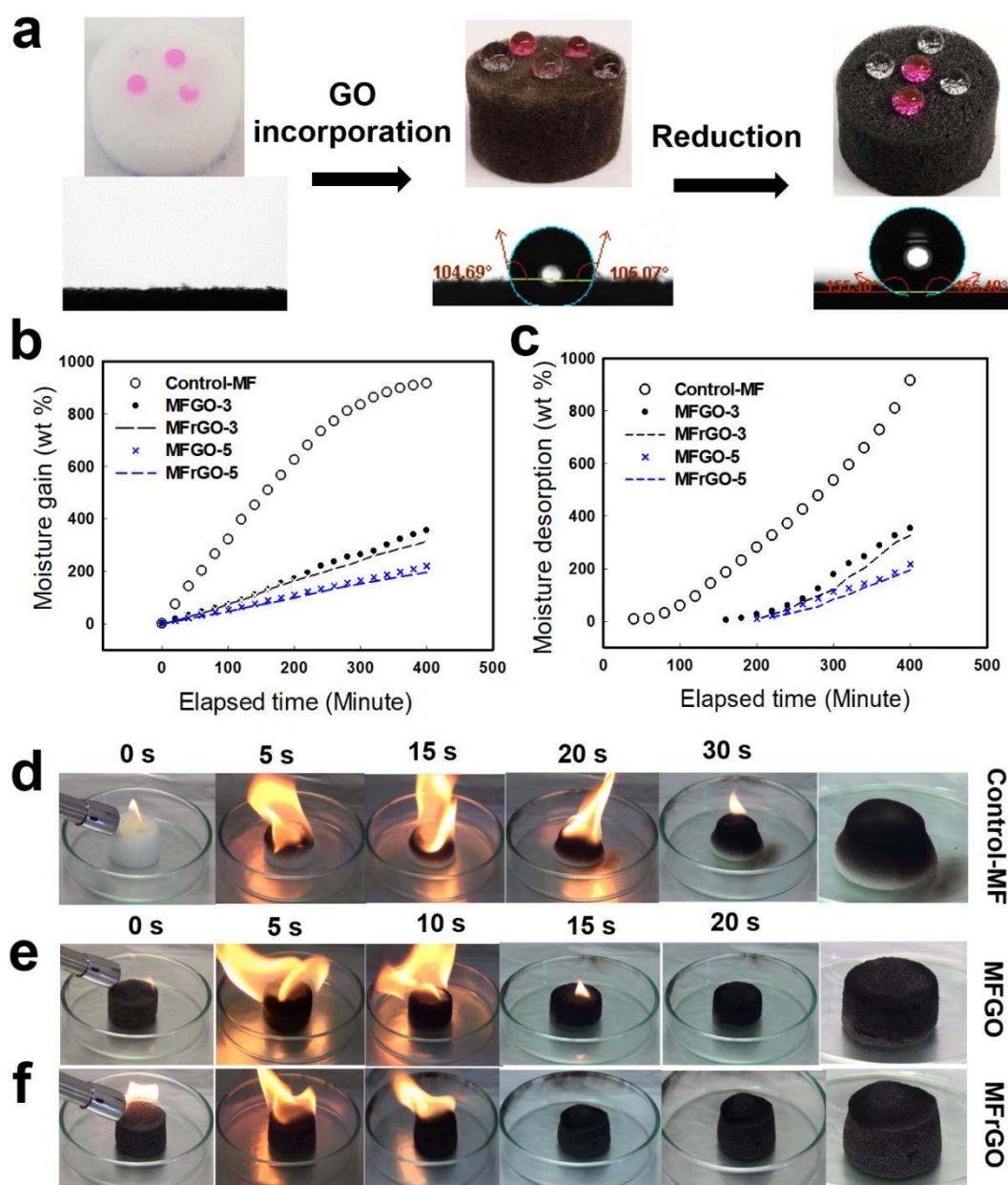
Figure 5. Wettability, mist absorption/desorption and flammability of the samples before and after reduction. a) Change in wettability of Control-MF, MFGO-3 and MFrGO-3 samples. (b and c) Mist absorption and desorption of MFGO and MFrGO samples compared to Control-MF. (d, e, and f) Digital photographs of the burning test showing high temperature stability and fire-retardant properties of the samples in the presence of gasoline (10 μl). d) Control-MF. e) MFGO-3. f) MFrGO-3.

Table of Contents and Figure:

A robust and light density lamella structure is developed based on self-assembly of GO. The incorporation of this unique structure into an open cell network showed maximum ~60.3 % enhancement in acoustic absorption between 128 Hz and 4000 Hz. The moisture insulation and fire-retardancy reinforce their functionality to be used in adverse environments including high humidity, under water and fire risks conditions.
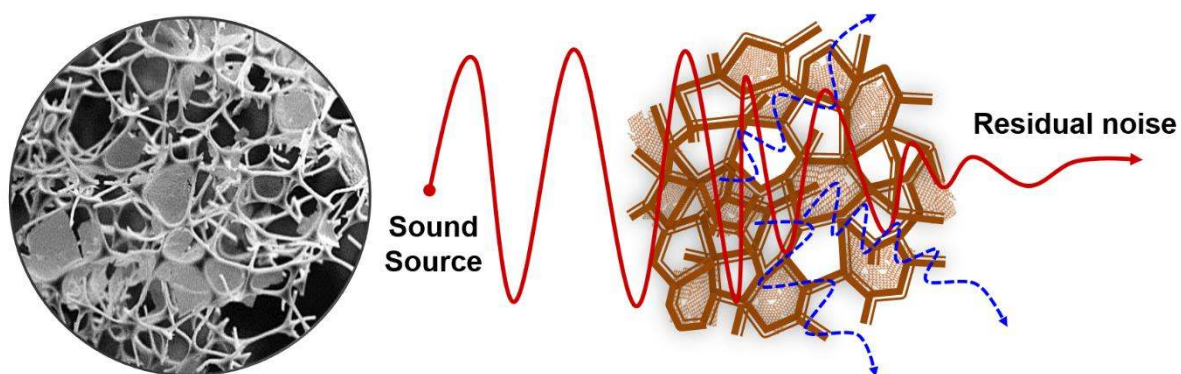
Supporting Information

Graphene oxide based lamella network for enhanced sound absorption

Md J. Nine[1,2], Md Ayub[3], Anthony C. Zande[3], Diana N.H. Tran[1,2], Benjamin S. Cazzolato[3], Dusan Losic[1,2]*

[1]School of Chemical Engineering, The University of Adelaide, Adelaide, SA 5005, Australia

[2]ARC Research Hub for Graphene Enabled Industry Transformation, *The University of Adelaide, Adelaide, SA 5005, Australia*

[3]School of Mechanical Engineering, The University of Adelaide, Adelaide, SA 5005, Australia

*Email address: dusan.losic@adelaide.edu.au

4. Materials and Method: (Supporting information)

Materials. Graphite flakes from Uley (Eyre Peninsula, Australia) were milled into a fine powder using a bench top ring mill (Rocklabs, New Zealand) for chemical exfoliation. Phosphoric acid (85%, H_3PO_4, chem-supply), 30% hydrogen peroxide (H_2O_2, chem-supply), ethanol (Chem-Supply), dimethylformamide (DMF, chem-supply), potassium permanganate ($KMnO_4$, Sigma–Aldrich), 98% sulfuric acid (H_2SO_4, Sigma–Aldrich) and 35% hydrochloric acid (HCl, Merck, Australia) were used as received. Milli-Q water (Purelab option-Q) was used in all aqueous solutions. Melamine foam with an apparent density of ~9.84 ± 0.2 g/cm^3 have been collected from local source, Bunnings Warehouse, South Australia.

Mechanical Compression Test and Measurement of Flow Resistivity. Mechanical compressibility of the samples was significantly dependent on their density. The apparent densities of the samples were measured according to ASTM D 1622-08 for 5 samples of each type after moisture conditioning at 25°C for 24 hrs. Mechanical compression test of the samples was performed using a Tensile/Compression/Bending tester (Deben, 200N, UK). The

speed of the jaw was set as 1.5 mm/minute for gradual compression under different compression length.

A specially designed standard (ASTM C-522) experimental setup was used to measure the static airflow resistance of each samples as illustrated in **Figure S11**. The ASTM C-522 standard is a direct airflow method in which unidirectional airflow is passed through test specimen to create pressure difference between upstream and downstream flow to measure the resulting pressure drop between two free faces of specimen in a tube.[1] The test rig consists of an acrylic tube connected to a line of compressed air with pressure regulator, flowmeter, and manometer. The specimen was mounted on an acrylic tube attached to the compartment. A digital manometer (475 Mark III, Dwyer, USA) is used to measure the pressure drop of airflow across the installed specimen after the flow has reached a steady stage. The resistance of airflow was defined here as the specific airflow resistivity (σ) per unit thickness (l) which is obtained using the following Equation-1.

$$\sigma = \frac{P_1 - P_2}{Ul/A} \tag{1}$$

where, P_1, P_2 are upstream and downstream static pressure to calculate pressure drop across the sample of l thickness and cross-sectional area of A, whereas flowmeter provides a volumetric flow rate (U) of air.

Acoustic Absorption Measurement Technique. The normal-incidence acoustic absorption coefficient of the Control-MF, MFGO, and MFrGO samples was measured in an impedance tube using two microphones in accordance with the ASTM E1050 standard.[2] A custom-made steel impedance tube with an internal diameter of 25.4 mm was used to measure the normal incidence acoustic absorption coefficient of the absorber samples. The impedance tube setup consists of a compression driver, a simple holder and a pipe section made of copper tube which holds the two microphones that measure the acoustic pressure in the tube. A photograph of the experimental apparatus with identified sections is shown in **Figure S12**.

The instrumentation compromised two ¼-inch Brüel & Kjær (B&K) array microphones type 4958, a four channel B&K Photon+^{TM} data acquisition system and LDS Dactron software. The B&K microphones have a free field frequency response (re 250Hz) of ± 2dB within the frequency range 50Hz to 10kHz. A pistonphone calibrator (B&K type 4230) was used to calibrate the microphone sensitivity to 94dB at 1 kHz. Measurement data was acquired with 4Hz frequency resolution, with a sampling interval of 7.6 μs (with 12800 lines and 32768 points) and sample records of finite duration of approximately 106 s for 300 averages.

The acoustic activity (normalized absorption coefficient, α) of the samples over a broad range of frequency spectrum between f_1 = 128 Hz to f_2 = 4000 Hz was also calculated to justify the effectiveness of the lamella samples based on the loading percentage of GO in the melamine skeleton. The normalized acoustic activity (α) was calculated using the following equation-2.[3,4]

$$\alpha_{normalized} = \frac{1}{(f_2 - f_1)} \int_{f_1}^{f_2} \alpha\,(f)\,df \qquad (2)$$

where, α (f) is frequency dependent absorption coefficient, f_1 and f_2 represent the lower and upper frequency limit at which the activity is calculation.

Moisture absorption and flammability test. The as-prepared samples of Control-MF, MFGO-3, MFGO-5, MFrGO-3, and MFrGO-5 were placed 20 mm apart from the mouth of mist generator (commercial humidifier) for moisture absorption,[5] and left at 35% RH at a temperature of 25 °C for moisture desorption. The change of mass was monitored in every 10 min interval for both moisture absorption and desorption cycle. The samples of Control-MF, MFGO-3, and MFrGO-3 (diameter of 26.5 mm and length of 14 mm) were soaked with 10 μl of gasoline to set fire in order to test structural and thermal stability during fire.

Characterizations. A scanning electron microscope (SEM-FEI QUANTA 450, Japan) was used to analyse the surface morphology of the GO, melamine foam (MF) and MFGO based

lamella structures at an applied voltage between 20-30 kV. A high-resolution Philips CM200, Transmission Electron Microscope (TEM), Japan was used for imaging the exfoliated GO flakes at 200 kV. Vibrational stretching modes of different molecular bonds in the GO, melamine, and rGO were studied by Fourier transform infrared spectroscopy (FTIR) (Nicolet 6700 Thermo Fisher, USA). The X-ray diffraction (XRD) patterns were recorded using Rigaku-Miniflex 600, Japan with radiation of Cu K-alpha, for pristine graphite and graphene oxide. Raman spectra were taken using a HORIBA scientific instrument (LabRam HR800 Ev, Jobin Yvon, Horiba, France) for the GO film deposited on a microscope glass using 532 nm laser (mpc 3000) as the excitation source by a 50× objective. Thermogravimetric analysis (TGA) and Derivative Thermogravimetry (DTG) of GO was analyzed by a TA instruments (Q-500, Tokyo, Japan) in N_2 atmosphere from ambient temperature to 600 °C at a rate of 5 °C/min. Furthermore, thermogravimetric instrument was used for analysis the combustion behaviour of Control-MF, MFGO-3 and MFrGO-3 in air atmosphere from ambient temperature to 800 °C at a rate of 2 °C/min. Water contact angle (WCA) and supplementary videos were recorded using an Attension theta optical tensiometer (KSV instruments, Finland) and high definition video camera (Sony HDR-PJ260).

## 2. Results and Discussion: (Supporting information)

2.1. Chemical analysis of the materials and lamella structure: The exfoliated GO and their physical properties are shown in **Figure S1** by transmission electron microscope (TEM), scanning electron microscope (SEM) and atomic force microscope (AFM). TEM and SEM of GO sheets confirm the regular exfoliation with an average lateral length of 4 - 5 μm (area of ~ 20 μm^2), while the AFM justifies the thickness of a few layers of GO sheets. The typical crystal structure of prepared GO is shown in **Figure S2** where the relevant XRD peak was identified at a 2θ position of 10.93° (**Figure S2a**) giving a greater interlayer distance (8.072

Å) than that of graphite (3.357 Å) at a 2θ position of 26.56°.[6] The FTIR characteristic peaks for oxygen functional groups in the GO structure are observed at 3000-3500 cm^{-1} (broad) and 1410 cm^{-1} (narrow) for O-H stretching vibrations, at 1225 cm^{-1} and 1050 cm^{-1} for C-O (epoxy and alkoxy groups) stretching peaks and 1730 cm^{-1} indicates C=O (carbonyl and carboxyl groups) stretching vibrations (**Figure S2b**).[7] Moreover, the peaks at 1630 cm^{-1} and 1510 cm^{-1} correspond to the skeletal and in-plane C=C stretching vibrations of GO, respectively. The characteristic Raman peaks of GO were identified at 1345 cm^{-1} (D band for breathing mode of sp2 carbon) and at 1590 cm^{-1} (G band for graphitic sp^2-bonded carbon) with an intensity ratio (I_D/I_G) of approximately 1.17 (**Figure S2c**). Thermogravimetric analysis of GO in N_2 atmosphere showed a two-step mass loss for the removal of moisture (step-1) and oxygen functional groups (step-2) with a final residue of 40% of mass at a temperature of 600 °C as shown in **Figure S2d**.

The melamine skeleton used in this experiment has a density of 9.84 kg/m^3 with an approximate cell size of 0.01 mm^2 (**Figure 1c, d**) and porosity of >97% (**Figure S3a**). The physical interaction between cellular limbs and interconnected GO lamella sheets is presented in **Figure S3b**. The FTIR characteristic peaks of MF and GO-based lamella (MFGO) have been studied (**Figure S3c**) to reveal the responsible functional groups in melamine formaldehyde,[8] and GO that interact to build strong lamella structure. The broad band peak at 3327 cm^{-1} is for N–H stretching vibration of secondary amines, the peaks at 1456 and 1323 cm^{-1} relate to asymmetrical and symmetrical methylene C–H bending, peaks at 1151 cm^{-1} and 1109 cm^{-1} correspond to C–N and C–O stretching vibrations, respectively, and the bands at 991 cm^{-1} and 810 cm^{-1} relate to C–H deformation vibrations, and the triazine ring is for out of plane vibration, respectively.[8-9] However, the incorporation of GO in the MF structure decreases the intensity of the characteristic peaks with a disappearance of the peak at 2951 cm^{-1} corresponding to the C–H (aliphatic) stretching. The further reduction of the sample

confirmed the disappearance of the oxygen functional groups in MFGO structure (compared with GO structure) as shown in **Figure S4a**. More importantly, the physical structure of the reduced lamella sample (MFrGO) has been observed to be similar as the non-reduced sample (MFGO) confirmed by SEM image in **Figure S4b** and **S4c**.
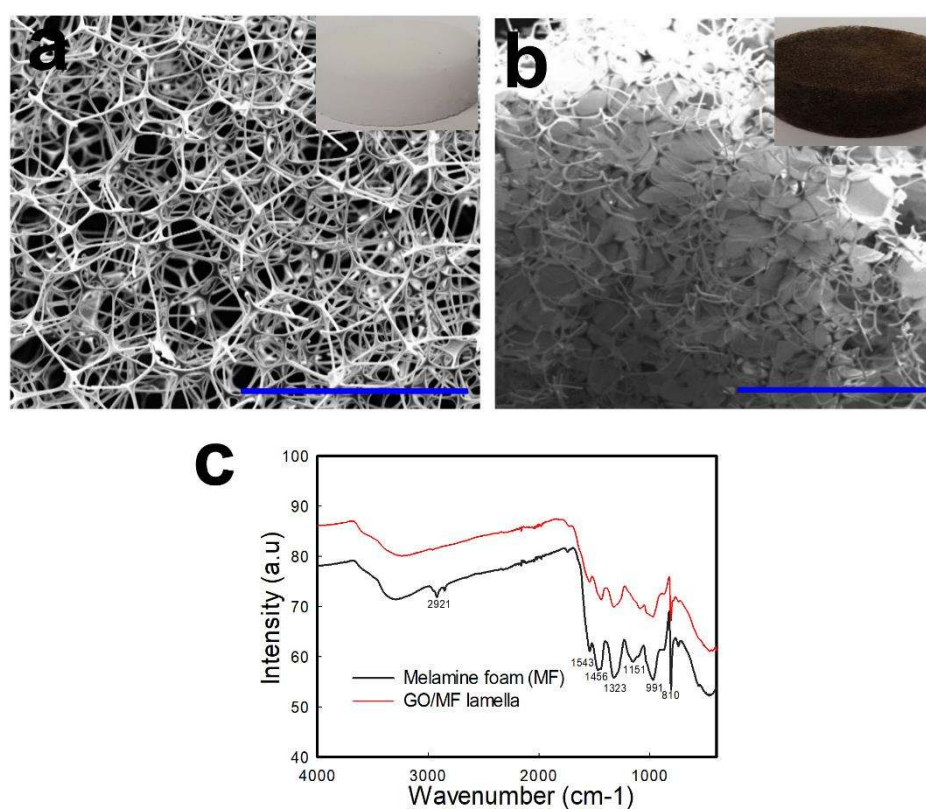
Supporting figures:
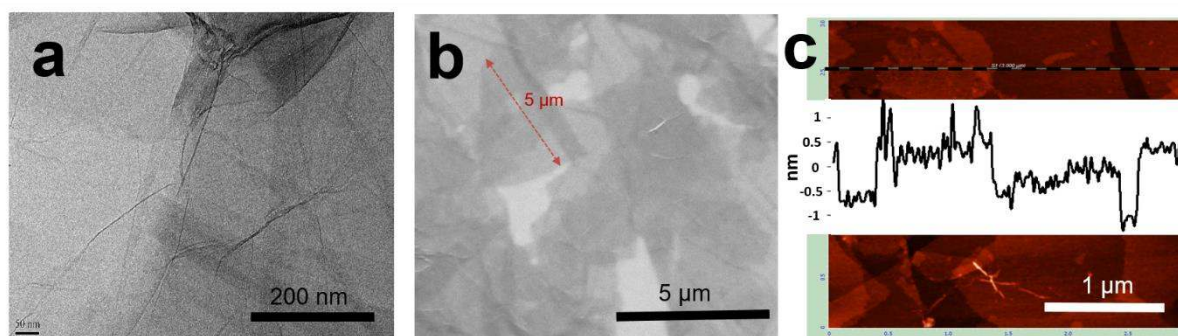
**Figure S1**. Exfoliated graphene oxide (GO). a) TEM. b) SEM scattered GO sheets overlapped. c) AFM of GO indicating few atomic layers.
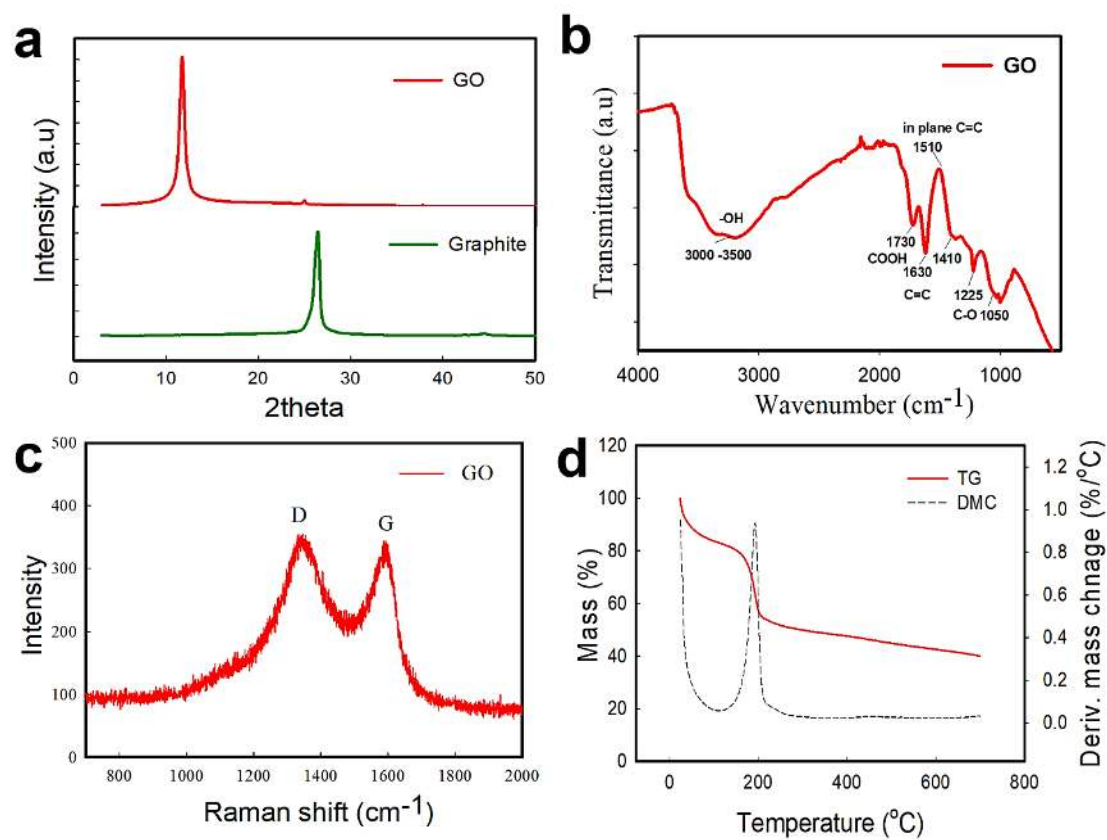
Figure S2. Chemical properties of exfoliated GO. a) XRD. b) FTIR. c) Raman. d) TGA of

GO in N₂ atmosphere.

Figure S3. Melamine foam before and after GO incorporation with open cell and closed cell structures. a) SEM image of Control-MF (Inset-photograph of Melamine foam). b) SEM image of MFGO-5 (Inset-photograph of MFGO-5). c) FTIR spectra of Control-MF and MFGO-5. Scale bar of a) and b) are 500 µm.
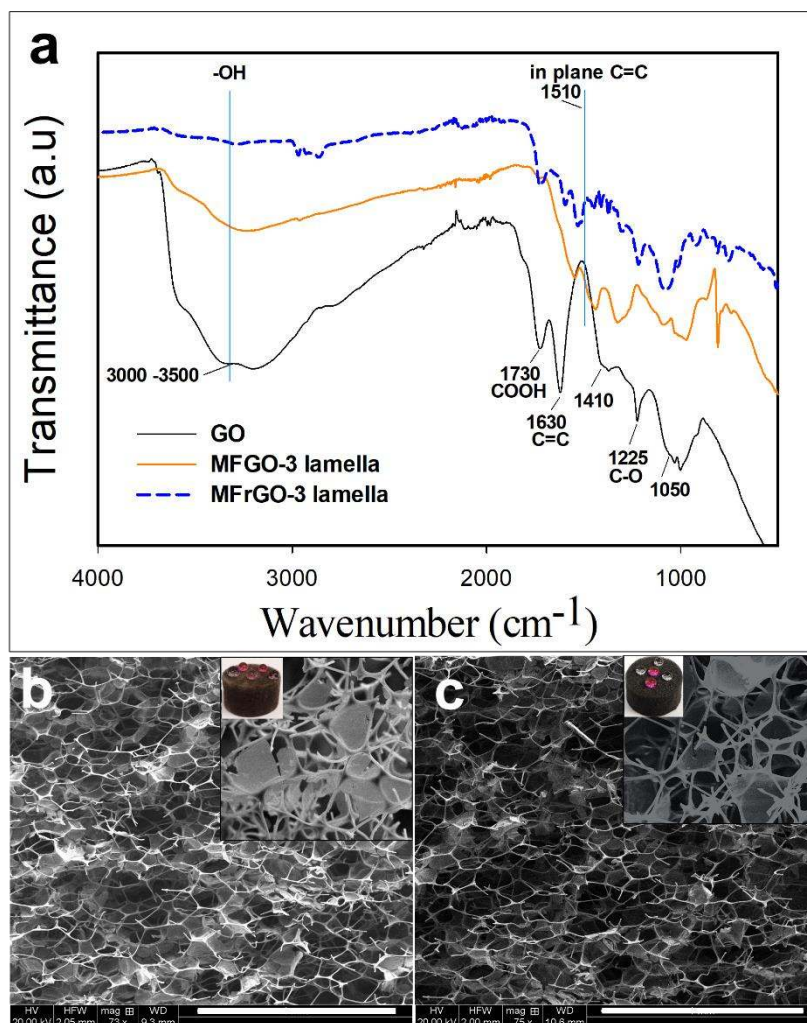
**Figure S4**: Chemical and physical structural variation before and after reduction of samples.

a) FTIR spectra of GO, MFGO-3 and MFrGO-3. b) SEM of MFGO-3. c) SEM of MFrGO-3.
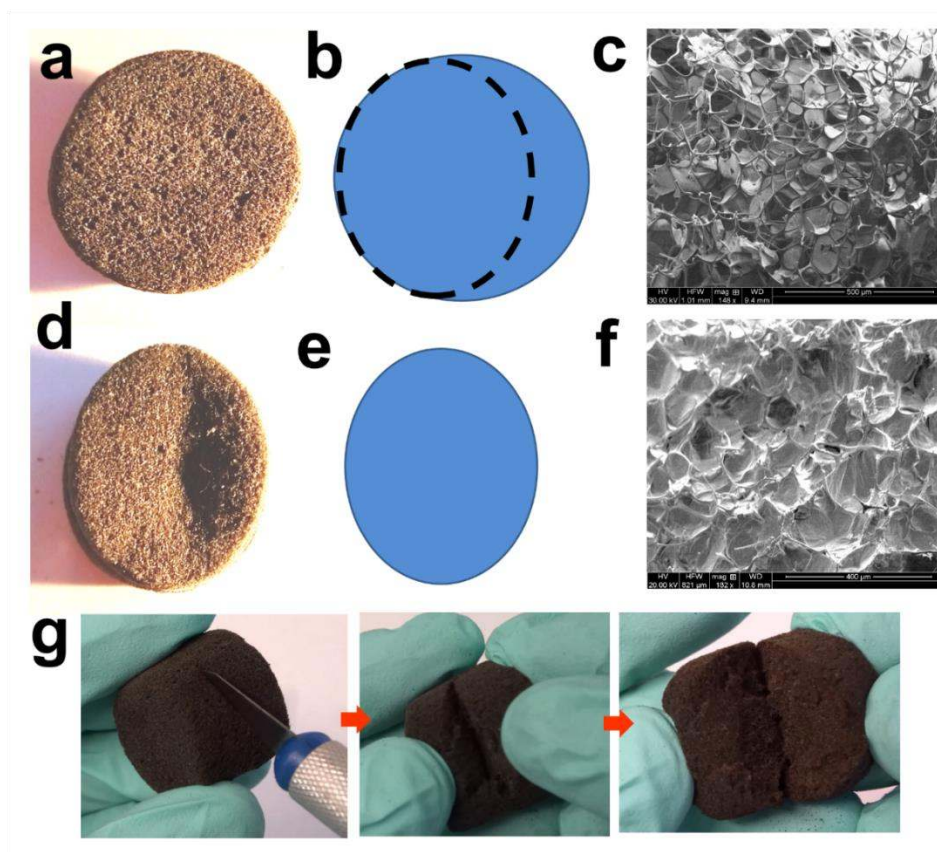
Figure S5. Critical loading of GO and volume contraction. (a, b and c). Photograph and SEM image of sample with maximum loading of GO in MF without significant shrinkage and deformation at an apparent density of 24.12 kg/m^3. (d, e and f) Photograph and SEM image of deformed structure affected by high loading of GO with an apparent density of 39.27 kg/m^3. g) Homogeneous loading of GO in the MF skeleton.
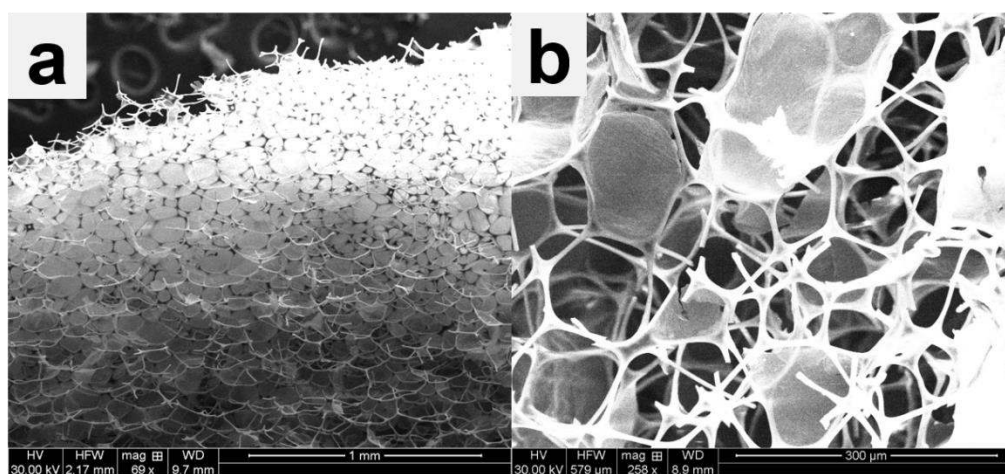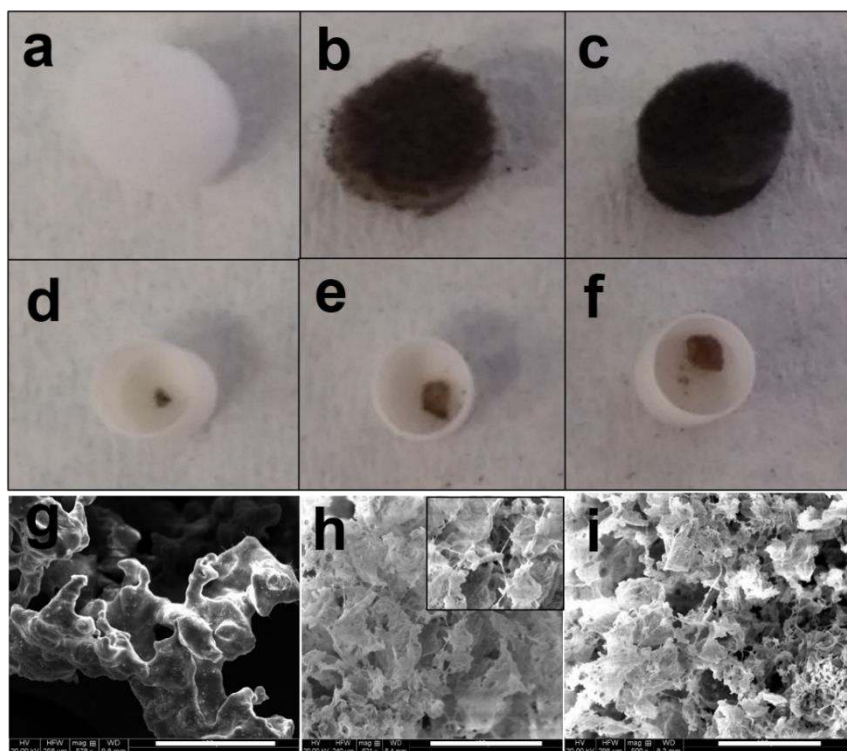
**Figure S6**. a) Low and b) high magnification of interconnected lamella structure.
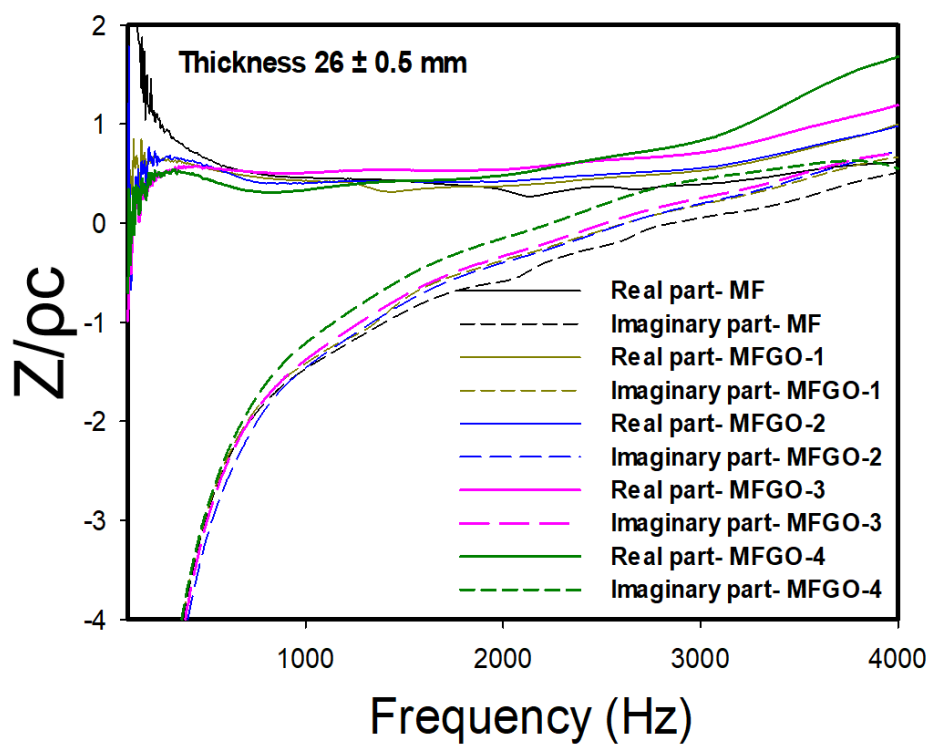
Figure S7. Acoustic impedance for the control-MF and GOMF lamella structures.
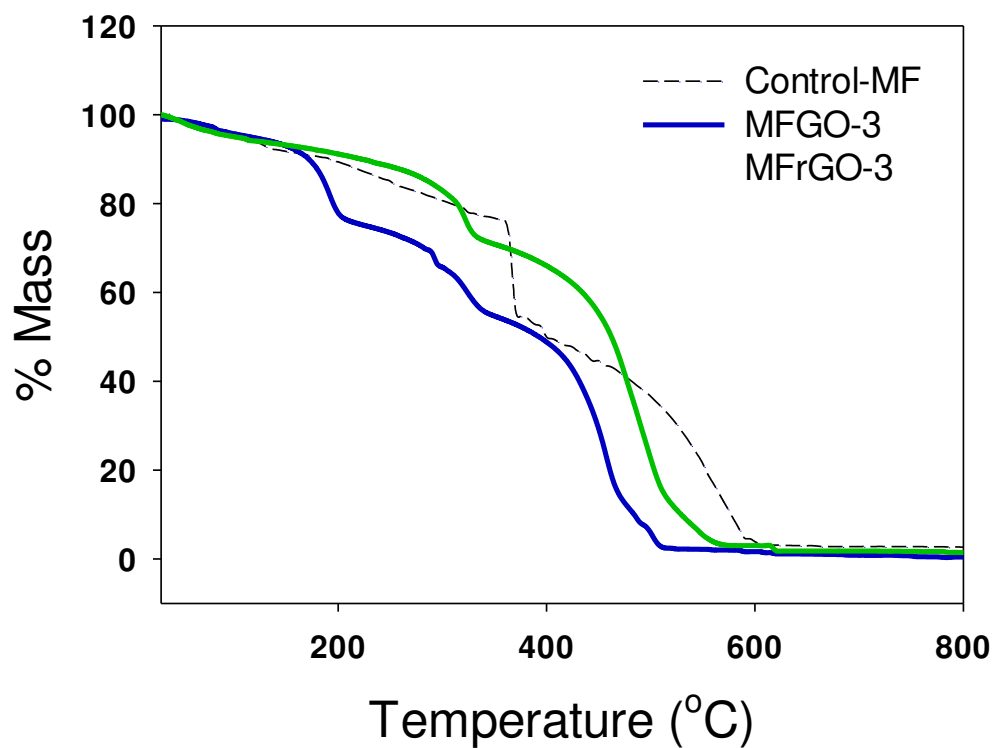
Figure S8. TGA of the samples to determine thermal stability of the structures in air atmosphere.
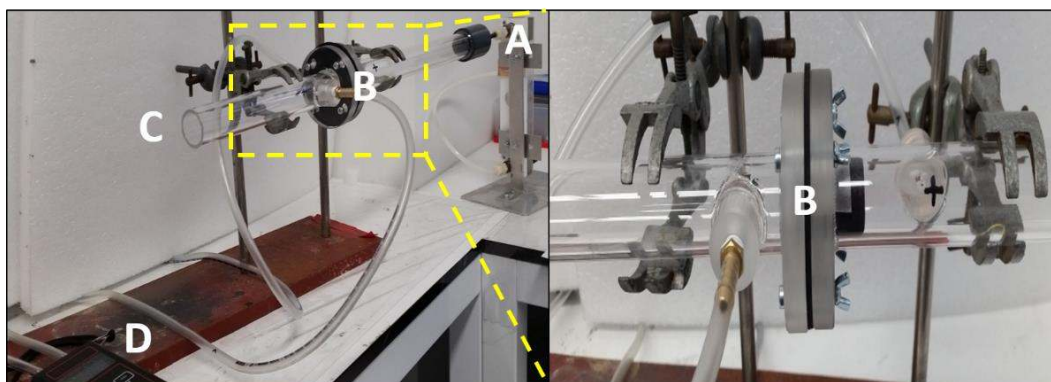
Figure S9. Char analysis of the samples after combustion. a) Control-MF. b) MFGO-3. c) MFrGO-3. d) Volume of Control-MF residue. e) Volume of MFGO-3 residue. f) Volume of MFrGO-3 residue. g) SEM image of Control-MF char. h) SEM image of MFGO-3. i) SEM image of MFrGO-3.
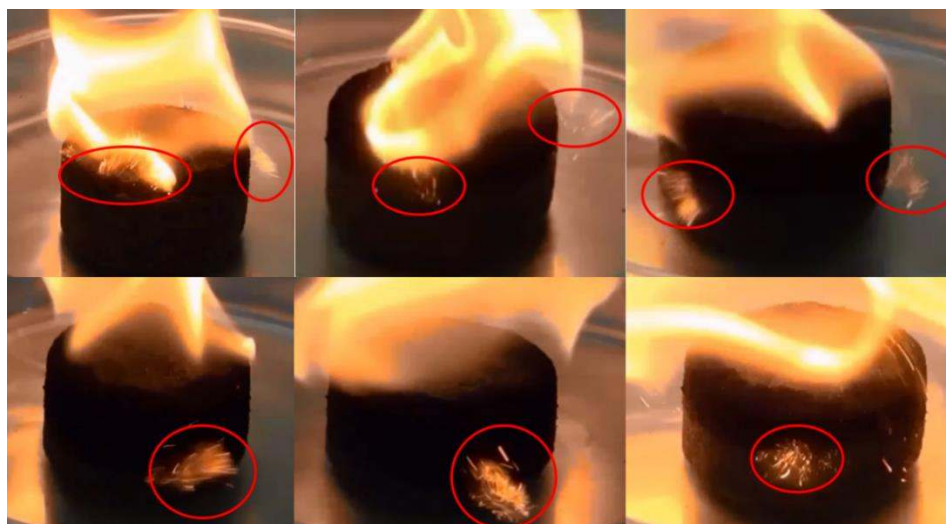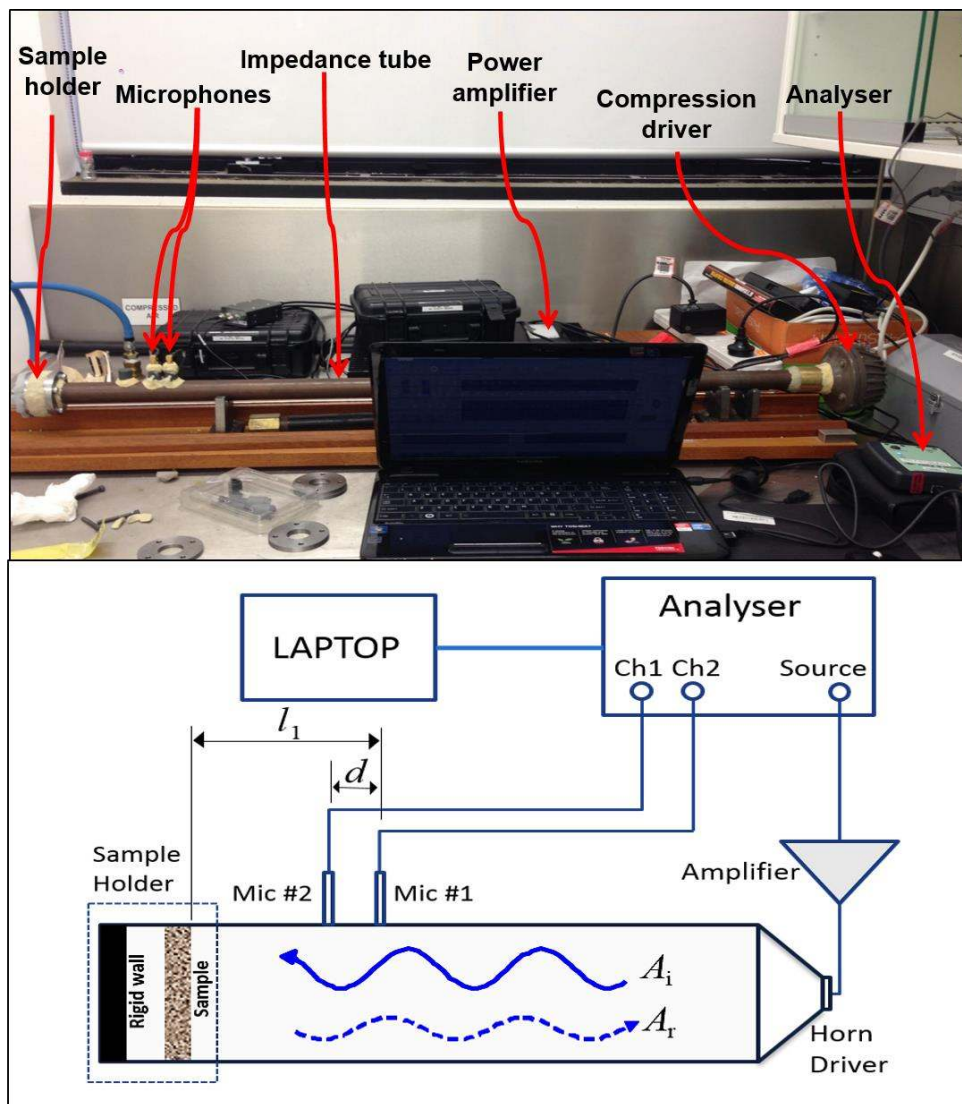
Figure S10. Series of small explosions captured in the MFGO structure while burning (marked in red ellipse).

Figure S11. Flow-resistance measurement set-up. Inset sections- A) Flowmeter, B) Sample compartment, C) Acrylic tube, D) Digital manometer.

Figure S12. Experimental setup and schematic presentation of acoustic absorption

measurement system.

Table S1. Physical properties of samples and acoustic activity under a broad range of frequency between 128 and 4000 Hz.

Specimen	Thickness (mm)	GO loading (wt%)	Density (kg/m^3)	Flow resistivity (σ) (kN.s/m^4)	Acoustic activity (α)	% increase in acoustic activity
Control-MF	6.5 ± 0.2	0	9.84	10.45 ± 0.84	0.131	---
	13.3 ± 0.2				0.281	---
	20 ± 0.5				0.450	
	26 ± 0.5				0.491	---
MFGO-1	6.5 ± 0.2	33 ± 3	12.39	18.92 ± 0.87	0.138	5.3
	13.3 ± 0.2				0.314	11.7
	20 ± 0.5				0.523	16.2
	26 ± 0.5				0.582	18.5
MFGO-2	26 ± 0.5	65 ± 2	15.68	--	0.661	34.6
MFrGO-2			12.71	--	0.646	31.5
MFGO-3	26 ± 0.5	95 ± 2	18.77	27.42 ±1.66	0.720	46.6
MFrGO-3			14.81	25.08 ±1.25	0.698	42.1
MFGO-4	26 ± 0.5	117 ± 2	21.41	--	0.748	52.3
MFrGO-4			16.19	--	0.732	49.1
MFGO-5	26 ± 0.5	145 ± 1	24.12	41.28 ±2.28	0.787	60.3
MFrGO-5			18.09	37.68 ±1.26	0.771	57.0

Supporting Movies:

Movie S1: Mechanical compressibility and homogeneity of GO distribution in the MF structure.

Movie S2: Wettability of Control-MF, MFGO and MFrGO samples.

Movie S3: Flammability of Control-MF, MFGO and MFrGO samples.

References.

[1]   In ASTM C522-03, Standard Test Method for Airflow Resistance of Acoustical Materials, *ASTM International, West Conshohocken, PA* **2003**.

[2]   J. Y. Chung, D. A. Blaser, *The Journal of the Acoustical Society of America* **1980**, 68, 907.

[3]   S. Basirjafari, R. Malekfar, S. E. Khadem, *Journal of Applied Physics* **2012**, 112, 104312.

[4]   R. Verdejo, C. Saiz-Arroyo, J. Carretero-Gonzalez, F. Barroso-Bujans, M. A. Rodriguez-Perez, M. A. Lopez-Manchado, *European Polymer Journal* **2008**, 44, 2790.

[5]   H. Viitanen, J. Vinha, K. Salminen, T. Ojanen, R. Peuhkuri, L. Paajanen, K. Lähdesmäki, *Journal of Building Physics* **2009**, 33, 201.

[6]   H.-J. Shin, K. K. Kim, A. Benayad, S.-M. Yoon, H. K. Park, I.-S. Jung, M. H. Jin, H.-K. Jeong, J. M. Kim, J.-Y. Choi, Y. H. Lee, *Advanced Functional Materials* **2009**, 19, 1987.

[7]   a) M. J. Nine, M. A. Cole, L. Johnson, D. N. H. Tran, D. Losic, *ACS Applied Materials & Interfaces* **2015**, 7, 28482; b) T. T. Tung, J. Yoo, F. K. Alotaibi, M. J. Nine, R. Karunagaran, M. Krebsz, G. T. Nguyen, D. N. H. Tran, J.-F. Feller, D. Losic, *ACS Applied Materials & Interfaces* **2016**, 8, 16521.

[8]   D. J. Merline, S. Vukusic, A. A. Abdala, *Polym J* **2013**, 45, 413.

[9]   S. Magina, M. Santos, J. Ferra, P. Cruz, I. Portugal, D. Evtuguin, *Materials* **2016**, 9, 100.